Power System Technology
Volume 50, No. 1, 2026
ISSN: 1000-3673

Transient Stability and Fault Current Analysis of a Nigerian Grid

.

Ezekiel Nnamere Aneke[1], Mamah Rotenna Ovid[2], Egbonwonu Livinus Emmanuel[3], Anthony Lordson Amana[4], Fidelis Ikechukwu Onah[5]

[1,3]Department of Electrical and Electronic Engineering, State University of Medical and Applied Sciences, Igbo-Eno, Enugu, Nigeria

[2,4,5]Department of Computer Engineering, Veritas University, Abuja, Nigeria

Abstract

The increasing fault current levels and transient instability challenges in modern power transmission networks pose significant threats to system reliability and operational security. To mitigate these challenges in the Nigerian 330 kV transmission network, this study investigates the impact of inertia and damping coefficients on fault current reduction and transient stability enhancement through the integration of shunt reactors. A multi-machine swing equation model was employed to analyze the dynamic behaviour of synchronous generators and evaluate the effect of shunt reactor integration under three-phase fault conditions. The analysis was conducted in the MATLAB R2023a environment using the Southern Nigerian 16-bus, 330 kV transmission network.

The results indicate that network reconfiguration with shunt reactor integration significantly improved rotor angle stability, rotor speed deviation, fault current performance, and overall system damping characteristics. For rotor power angle and rotor speed deviation analyses, Generators 1, 2, 4, and 5 exhibited superior damping properties in both existing and reconfigured network configurations, with oscillatory responses diminishing over time. In contrast, Generators 3 and 6 in the existing network demonstrated inadequate damping and were more susceptible to instability. Following reconfiguration, these generators showed substantial improvements in dynamic performance, resulting in reduced rotor angle deviations, enhanced damping, and improved synchronization across the network. The findings suggest that network reconfiguration enhances transient stability by mitigating excessive rotor speed deviations and preventing phase drift among generators.

Fault current analysis revealed significant reductions across all generating units after shunt reactor integration. Notably, the fault current of Generator 1 decreased from 4.5 p.u. to 2.5 p.u., while Generator 2 experienced a reduction from 3.5 p.u. to 2.0 p.u. The most significant stability improvements were observed in Generators 3 and 6, which previously exhibited poor damping characteristics. Furthermore, sensitivity analysis showed that the peak fault current occurred at a reactor reactance X_Rt=0.00 pu.u., where the absence of additional reactance minimized network impedance and allowed maximum current flow. As reactor reactance increased, fault current levels progressively decreased, reaching approximately 0.8 p.u. at X_Rt=0.50 pu.u. and 0.6 p.u. at X_Rt=0.75 pu. These results confirm an inverse relationship between reactor reactance and fault current magnitude, demonstrating that higher reactance effectively limits fault current and enhances system protection.

The study concludes that appropriate inertia and damping characteristics, combined with shunt reactor compensation, significantly improve transient rotor angle stability, suppress excessive rotor speed deviations, reduce fault current levels, and enhance the overall resilience and security of the Nigerian 330 kV transmission network under severe fault conditions.

Key Words: Inertia Coefficient, Damping Coefficient, Fault Current Reduction, Transient Stability, Rotor Angle Stability, Rotor Speed Deviation, Shunt Reactor, Multi-Machine Power System, Nigerian 330 kV Transmission Network.

1. Introduction

Power system stability is the most critical area of study for ensuring the reliable and efficient operation of power networks. This study involves analysing the system's behaviour under various disturbances and operating conditions to prevent blackouts or total system failure. As highlighted in [1], these disturbances can stem from sudden load disconnections, line switching operations, equipment malfunctions, abrupt transmission line interruptions, transformer or generator failures, vandalism, and other incidents. If such issues are not promptly addressed, they can lead to widespread power outages and significant damage to system components. Power system stability is broadly categorized into three types: dynamic, transient, and steady-state stability. Transient stability refers to the power system's ability to respond to major disturbances that cause notable changes in rotor speeds, power angles, and power transfers. As described in [2], this phenomenon occurs over a short duration, typically within seconds. In modern power system analysis and control, transient stability is a crucial factor for maintaining operational reliability. Stability in the synchronization of the several synchronous generators across the power system is necessary to maintain functional security. One way to ensure proper network fortification is to have a well-damped and higher inertia of the network's generators. According to [3], depending on how the system is configured, the generator rotor angles may oscillate, converge, or diverge when a glitch occurs. When the defect is fixed, machines can restore synchronism because proper damping stops oscillations from growing. Unstable machines with inadequate damping result in rotor angles that are constantly diverging. When the issue is fixed, the system becomes more unstable and faster. Recently, the Nigerian power system has faced several threats of system failures and loss of synchronism owing to various issues, including a weakened network, vandalism, banditry, and fuel shortages, and so on. It is necessary to analyse the impact of inertia and damping coefficients on the fault current and transient power angle stability of the network generators.

Transient stability is a critical aspect of modern power system analysis and control, ensuring reliable operation under dynamic conditions. According to [1], factors such as fault type, fault location, and network configuration significantly impact transient stability. Traditional time-domain simulation techniques for transient analysis, as highlighted in [4], are computationally demanding and require precise network modeling for accurate results. To address these challenges, [5] proposed an imbalance correlation method using support vector machines to evaluate the transient stability of the IEEE 39-bus system and the Eastern China Power Network. While this approach demonstrated promising results, its effectiveness was constrained by the limitations of the training dataset. The adoption of an adaptive grouping strategy was suggested to improve logical coherence and analytical insights. In [6], a graph attention network (GAN)-based approach was employed to analyze instability in Northeast China's power systems, leveraging the grid's architecture for enhanced modeling. This method effectively identified transient rotor angle instability and short-term voltage instability, surpassing the performance of traditional graph convolutional networks. However, the study did not consider variations in rotor angle stability resulting from differing inertia and damping coefficients, leaving room for further investigation. References [7], [8], [9], and [10] have provided valuable insights into transient stability and fault current issues in power systems. Reference [7] introduced an online monitoring system to assess transient stability in real-time, offering early warnings of instability. Their approach utilized vision-transformer-based techniques to identify unstable generators and evaluate transient stability, coupled with an adaptively updated instability criterion. In [8], the authors examined transient power angle and fault current behavior in virtual synchronous generators to address instability and fault-overcurrent challenges. They proposed a transient power angle stability analysis method that incorporated real power reference adjustments and reactive voltage regulation coefficients, enabling adaptive responses and suppressing fault currents. However, this study did not analyze the effects of inertia and damping coefficients on transient power angle stability and fault currents or consider their control methods. Reference [9] emphasized the need to reduce the critical fault clearance time to prevent system blackouts in the Nigerian power grid, while [10] highlighted the importance of rapid relay and circuit breaker responses to faults. Despite these contributions, both studies failed to explore the impact of inertia and damping coefficients on fault currents, transient power angle stability, and control strategies. This research aims to address these gaps by enhancing transient power angle stability and mitigating fault currents in the Nigerian Southern-region 16-bus, 330kV power system network, and utilizing shunt reactors as a solution. Historically, shunt reactors have been widely utilized in high-voltage transmission networks to compensate for excess reactive power generated by long transmission lines and lightly loaded systems. Their application helps in maintaining acceptable voltage profiles, reducing over-voltage conditions, and enhancing overall power system operational stability. In large interconnected power systems, shunt reactors are commonly introduced to absorb reactive power and mitigate the Ferranti effect, particularly in extra-high-voltage transmission corridors. While most previous studies have primarily considered shunt reactors for voltage regulation and reactive power compensation purposes, the present study extends their application by investigating their impact on transient performance enhancement. Specifically, this study employs shunt reactors as a network reconfiguration tool for fault current limitation and rotor angle damping enhancement in the Southern Nigerian 16-bus network. This approach differs from conventional applications by emphasizing transient power-angle stability and synchronization improvement under disturbance conditions.

2. Methodology

2.1 Description of the Network

The 16-bus, 330kV power system network in the southern region of Nigeria consists of six synchronous generator buses and eleven load buses. A single-line diagram of the network is illustrated in Figure 1. The system includes 18 branches connecting the buses, with shunt reactors installed at specific bus locations, namely Makurdi, Lafia, and Benin. The network was modeled using PSAT 2.1.11, and the analysis was conducted in MATLAB R2023a. Steady-state load flow analysis was performed using the AC Newton Raphson's power flow method within the MATPOWER 8.0 environment. The load data, generator data, line data, and generator dynamic parameters were gathered from the Transmission Company of Nigeria (TCN).

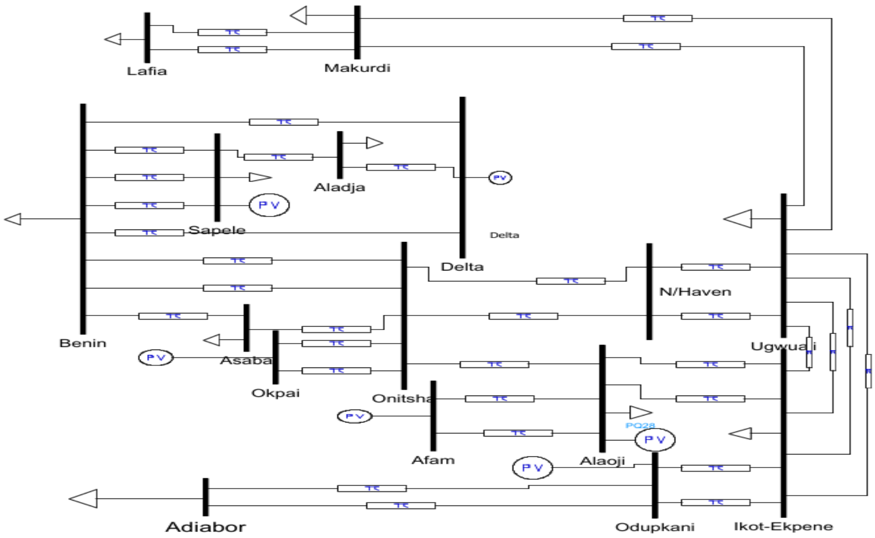

Figure 1: Single line diagram of the southern Nigerian power network

2.2 Mathematical Derivation of the Swing Equation for Multi-Machine Grid Network

Assuming the torques operating on the machine rotor are unbalanced, the overall torque stimulating acceleration or deceleration may be calculated as demonstrated in [11]:

$$T_{accel} = T_{Mech} - T_{Elect} \quad (1)$$

Where

T_{accel} is the accelerating torque

T_{Mech} is the mechanical torque

T_{Elect} is the Electromagnetic torque

If the retarding torques are neglected because of the rotational losses.

Then

$$T_{mech}.\omega_s - T_{elect}.\omega_s = P_{mech} - P_{elect} = P_{accel} \quad (2)$$

Where

ω_s is the synchronous speed of the generator

P_{Mech} is the mechanical power

P_{Elect} is the electromagnetic power

P_{accel} is the accelerating power

The swing equation of a synchronous generation is given as shown in Kundur [12]:

$$\frac{2H}{\omega_s}\frac{\partial^2\delta}{\partial t^2} = P_{mech} - P_{elect} - \frac{D_k}{\omega_s}\frac{\partial\delta}{\partial t} \quad (3)$$

Where

D_k is the damping coefficient in per unit and δ is the angle of the synchronous generator

By using the per unit value of $\bar{t}$ in equation (3) above yields

$$2H\omega_s\frac{\partial^2\delta}{\partial \bar{t}^2} = P_{mech} - P_{elect} - D_k\frac{\partial\delta}{\partial \bar{t}} \quad (4)$$

Therefore

$\bar{J} = 2H\omega_s = 4\pi f H$ is the per unit moment of inertia

The inertia constant H, which shapes the turbine-generator's dynamic characteristics, is a critical generator parameter. The moment of inertia represents the influence of the combined spinning masses of the turbine and generator as stated [13].

Hence, the swing equation for damping becomes

$$2H\omega_s\frac{\partial^2\delta}{\partial \bar{t}^2} = P_{mech} - P_{Loss} - P_{elect} - D_k\frac{\partial\delta}{\partial \bar{t}} \quad (5)$$

Considering a multi-machine of k-bus system with m number of alternators at bus h. The steady-state analysis of the network performed prior to the onset of the fault yields the source voltage (E_h), the active power (P_{gh}) and the reactive power (Q_{gh}) of the generators and the voltage (V^*).

Therefore, the source voltage is given as demonstrated in [14]

$$E_h = V_h + jX_hI \quad (6)$$

Since $V = IZ; I = \frac{V}{Z}$

But the admittance, $Y = \frac{I}{Z}$

Hence

$$I = VY \quad (7)$$

Complex absolute power is given by

$$S^* = P_h - jQ_h = V_h^*I \quad (8)$$

$$I = \frac{P_h - jQ_h}{V_h^*} \quad (9)$$

Substitute equation (9) into equation (6)

$$E_h = V_h + jX_h\left(\frac{P_h - jQ_h}{V_h^*}\right) \quad (10)$$

Where

X_h is the reactance at bus h. Changing the load buses to form load admittance, Y_{Lh} at the bus.

Putting equation (7) into equation (8)

$$P_{Lh} - jQ_{Lh} = V^*VY = |V_h|^2Y_{Lh}$$

$$Y_{Lh} = \frac{P_{Lh} - jQ_{Lh}}{|V_h|^2} \quad (11)$$

Where

P_{Lh} *and* Q_{Lh} are the bus active and reactive load powers

The steady-state bus admittance matrix, inclusive of the generator's admittance and the converted load admittance, is given as

$$Y_{hbus} = \begin{bmatrix} Y_{11} & Y_{12} \\ Y_{21} & Y_{22} \end{bmatrix} \tag{12}$$

The output power of each generator is given as

$$P_{elect} = E_h^2 Y_{hh} cos\theta_{hh} + \sum_{\substack{h=1 \\ h \neq f}}^{m} |E_h||E_f||Y_{hf}|\cos(\theta_{hf} - \delta_h + \delta_f) \tag{13}$$

Utilizing equation (13), the output power during and after the fault condition will be determined using the swing equation given in equation (5).

$$2H\omega_s \frac{\partial^2\delta}{\partial \bar{t}^2} + D_k \frac{\partial\delta}{\partial \bar{t}} = P_{mech} - P_{Loss} - \left(E_h^2 Y_{hh} cos\theta_{hh} + \sum_{\substack{h=1 \\ h \neq f}}^{m} |E_h||E_f||Y_{hf}| \cos\left(\theta_{hf} - \delta_h + \delta_f\right) \right) \tag{14}$$

During fault condition, the swing equation is given as

$$2H\omega_s \frac{\partial^2\delta}{\partial \bar{t}^2} + D_k \frac{\partial\delta}{\partial \bar{t}} = P_{mech} - P_{Loss} - P_{elect(during\ fault)} \tag{15}$$

After Fault condition, the swing equation is express as follows

$$2H\omega_s \frac{\partial^2\delta}{\partial \bar{t}^2} + D_k \frac{\partial\delta}{\partial \bar{t}} = P_{mech} - P_{Loss} - P_{elect(after\ fault)} \tag{16}$$

The importance of damping and inertia coefficients for fault current and transient stability cannot be overstated. Higher coefficients improve grid network stability, whilst lower values lessen it.

2.3 Mathematical modelling of Critical Clearing Time and Angle

The machine system shown in Figure 2 below demonstrates the functioning of a synchronous generator of mechanical input power P_{mech} at a constant angle $\delta_0(P_{mech} = P_{elect})$, as stated in point 1 of Figure 3. When a three-phase short circuit defect occurs at point F, as illustrated in Figure 2, the electromagnetic power decreases to zero and the state point moves to point 2. As a result, positive acceleration causes the angle to grow, rendering the system unstable. That is, the state point increases from 2 to 3. At step three, the circuit breaker clears the problem on the transmission line. Thus, $P_{elect} = P_{max} \sin\delta$ it is routed to point 4. Figure 3 shows the rotor retards from points 4 to 5. At point δ_1, when $A_1 = A_2$ the operating system is said to be stable. However, if $A_2 < A_1$, then the system is unstable as presented in [15] and [11].

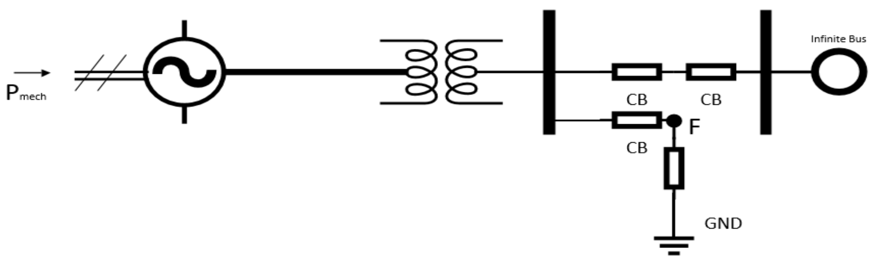

Figure 2: An infinite bus network [15]

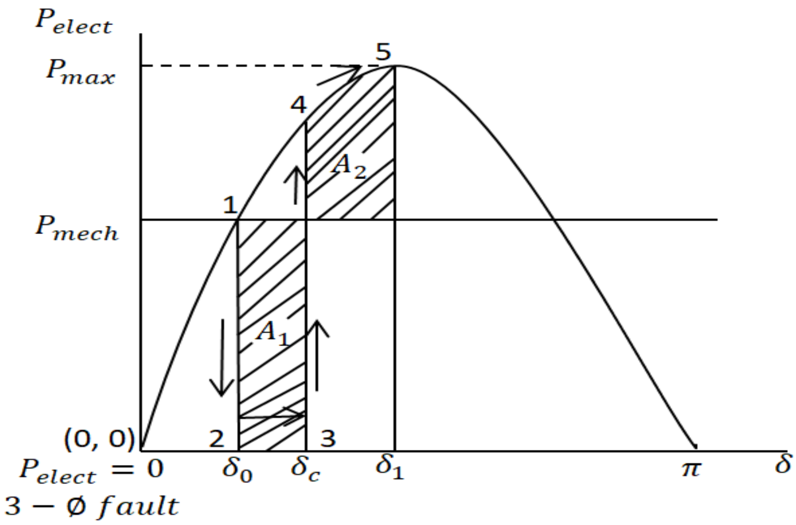

Figure 3: Electromagnetic power-angle Curve [15]

From figure 3, as shown in [15], during fault $P_{elect} = 0$ and

$$\delta_{max} = \pi - \delta_0 \qquad (17)$$

Whilst $P_{elect} = P_{max} \sin \delta$ (18)

The integral of the areas is given by

$$A_1 = \int_{\delta_0}^{\delta_{cr}} (P_{mech} - 0) d\delta = P_{mech}(\delta_{cr} - \delta_0) \qquad (19)$$

$$A_2 = \int_{\delta_{cr}}^{\delta_{max}} (P_{max} \sin \delta - P_{mech}) d\delta = P_{max}(cos\delta_{cr} - cos\delta_{max}) - P_{mech}(\delta_{max} - \delta_{cr}) \qquad (20)$$

Equating equations (19) and (20) yields

$$cos\delta_{cr} = \frac{P_{mech}}{P_{max}}(\delta_{max} - \delta_0) + cos\delta_{max} \qquad (21)$$

Replacing equations (17) and (18) into equation (21) will yield

$$\delta_{cr} = cos^{-1}[(\pi - 2\delta_0)sin\delta_0 - cos\delta_0] \qquad (22)$$

Equation (22) represents the critical clearing angle.

If the fault continuous, the swing equation is reduce to $P_{elect} = 0$

Hence,

$$\frac{\partial^2 \delta}{\partial t^2} = \frac{\pi f}{H} P_{mech} \qquad (23)$$

By double integration of equation (23)

$$t_{cr} = \sqrt{\frac{2H\delta_{cr} - \delta_0}{\pi f P_{mech}}} \qquad (24)$$

Equation (24) is referred as the critical clearing time.

2.4 Transient Stability Analysis Problem Formulation

The inertia and damping coefficients of a generator in dynamic state is represented as shown in equation (5). These coefficients are adjusted within the network generators to ascertain the impact of transient power angle stability and fault current.

The inertia constant H, as expressed in [15] is given by:

$$H = \frac{1/2 J\omega_r^2}{S_{Base}} \qquad (25)$$

where, ω_r denotes the angular displacement of the rotor; J is the moment of inertia of the generator and S_{Base} is the absolute power of the generator in MVA.

The Inertia coefficient is represented as:

$$M = \frac{J\omega_r}{S_{Base}} \tag{26}$$

where, M is the inertia coefficient and ω_r represents the generator angular speed.

The objective function is to minimize the rotor angle deviation. Subject to the following constraints:

i. Transient power angle stability

The power angle equation as expressed in [15] is shown as:

$$P_{elect} = \frac{E_g * V_{RE} sin\delta}{X} \tag{27}$$

where, δ is the power angle, $E_g\ and\ V_{RE}$ are the generator's internal voltage and receiving end voltage and X is the reactance of the generator and the transmission line reactance.

The swing equation for transient stability analysis is given in equation (28) where damping is reduced to zero.

$$2H\omega_s \frac{\partial^2 \delta}{\partial \bar{t}^2} = P_{mech} - P_{elect} \tag{28}$$

Substituting equation (27) into equation (28) will yield

$$2H\omega_s \frac{\partial^2 \delta}{\partial \bar{t}^2} = P_{mech} - \frac{E_g * V_{RE} sin\delta}{X} \tag{29}$$

Equation (29) represents the transient power angle stability equation. This will help determine the generator's responsiveness during a transient event.

For stability, $0^o < \delta < 90^o$.

ii. The Critical clearing angle and time equations: Are expressed in equations (22) and (24) above.

iii. Fault Current determination

This study employed a balanced fault type on network synchronous generators for both existing and reconfigured networks. The impact of adding a reactor to the network will be investigated. Rewriting equation (5) will result in

$$2H\omega_s \frac{\partial^2 \delta}{\partial \bar{t}^2} + D_k \frac{\partial \delta}{\partial \bar{t}} = P_{mech} - P_{Loss} - P_{elect} \tag{30}$$

Equation (30) when evaluated will be utilized to simulate the dynamics of the rotor angle at a three phase faults disturbance.

Considering a three phase fault, the fault current equation is obtained thus by [15]:

$$I_f = \frac{E_i}{\sqrt{3} \times X_d''} \tag{31}$$

where, I_f denotes the fault current, E_i is the internal voltage of the generator and X_d'' is the sub-transient reactance of the generator.

Evaluating equations (27) and (31) and substituting into equation (30) will yield

$$2H\omega_s \frac{\partial^2 \delta}{\partial \bar{t}^2} + D_k \frac{\partial \delta}{\partial \bar{t}} = P_{mech} - P_{Loss} - \frac{E_i}{X_d''} sin\delta \tag{32}$$

Equation (32) represents the swing equation of the existing network.

For the reconfigured network we have

$$2H\omega_s \frac{\partial^2 \delta}{\partial \bar{t}^2} + D_k \frac{\partial \delta}{\partial \bar{t}} = P_{mech} - P_{Loss} - \frac{E_i}{X_d'' + X_{Rt}} sin\delta \tag{33}$$

where, X_{Rt} is the added impedance (reactor) to the network.

The influence of inertia and damping coefficients can aid in network stabilization. To ensure the network's transient stability, an elevated level of inertia and damping is necessary; this reduces the rotor angle and the magnitude of oscillations.

iv. The transient power angle stability during and after disturbance is expressed as follows

During fault condition, the swing equation is given as

$$2H\omega_s \frac{\partial^2 \delta}{\partial \bar{t}^2} = P_{mech} - P_{elect(during\ fault)} \quad (34)$$

After Fault condition, the swing equation is express as follows

$$2H\omega_s \frac{\partial^2 \delta}{\partial \bar{t}^2} = P_{mech} - P_{elect(after\ fault)} \quad (35)$$

v. Operational constraints include the following

$$P_{Gi}(min) \le P_{Gi} \le P_{Gi}(\max) \quad for\ i = 1,2,3,\dots,l$$

$$|V_i|(min) \le |V_i| \le |V_i|(\max) \quad for\ i = 1,2,3,\dots,l$$

To mathematically validate the observed improvement in synchronization after network reconfiguration, a comparative assessment of critical clearing time (t_{cr}) was performed for the weakest generators (Generator 3 and Generator 6). The t_{cr} represents the maximum fault duration that can be tolerated before the generators lose synchronism.

Table 1 presents the comparative t_{cr} values obtained for both the existing and reconfigured networks.

Table 1: Critical Clearing Time comparison for weak generators

Generator	**Existing Network t_{cr} (s)**	**Reconfigured Network t_{cr} (s)**	**Percentage Improvement (%)**
Gen 3	0.31	0.44	41.94
Gen 6	0.28	0.42	50.00

The results indicate that the reconfigured network increases the critical clearing time of the weak generators, implying enhanced transient stability characteristics. An increase in critical clearing time allows the system to tolerate disturbances for longer durations before losing synchronism, thereby validating the observed improvement in rotor angle stability and synchronization behaviour.

3. Results and Discussion

3.1 Load Flow Analysis Solution

The load flow analysis of the Southern Nigerian 16-Bus system, conducted using the Newton-Raphson load flow method, is presented in Table 2. The bus voltage levels are within the acceptable range of 0.95 pu to 1.05 pu. The network's total losses are 14.043 MW and 117.51 MVAr, indicating that the system is operating efficiently and is in good condition.

Table 2: Load flow solution of the 16-bus southern Nigerian network

Bus Name	**Bus No**	**Voltage**		**Generation**		**Load**	
		Mag(pu)	**Ang(deg)**	**P(MW)**	**Q(MWAr)**	**P(MW)**	**Q(MWAr)**
Afam	1	1.000	0	236.14	131	153.3	55
Benin	2	0.998	4.023	0	0	135.3	50
Sapele	3	1.000	5.779	208	-27.79	0	0
Onitsha	4	0.995	1.742	0	0	182.7	60
Asaba	5	0.994	1.823	0	0	94.7	35
Delta	6	1.000	6.213	300.7	6.31	115.1	40
New/Haven	7	0.994	-1.23	0	0	169.6	60
Ugwuaji	8	0.995	-1.243	0	0	22.6	9
Makurdi	9	1.001	-4.557	0	0	94.7	35
Lafia	10	1.004	-4.945	0	0	22.6	7
Okpai	11	1.000	4.969	325.8	-9.14	0	0
Ikot-Ekpene	12	0.998	2.381	0	0	0	0
Alaoji	13	0.994	-0.29	0	0	443.3	100
Adiabor	14	0.999	7.339	0	0	40.6	15
Odukpani	15	1.000	7.46	463	-27.35	0	0

Aladja	16	1.000	5.899	0	0	45.1	15

3.2 Rotor Angle Stability of the Network

Figure 4 compares rotor angle stability between the existing and reconfigured systems across multiple network generators. Solid lines represent the existing system, while dashed lines denote the reconfigured system. In the current system configuration, generators exhibiting pronounced rotor angle growth, notably Generator 3 and Generator 6, demonstrate inadequate damping, which may precipitate instability. In contrast, generators in the reconfigured system often have lower rotor angle deviations, implying increased damping and synchrony. Specifically, Generator 6 in the existing system manifests an undamped response, characterized by a persistent increase in rotor angle, indicative of a potential loss of synchronism. Generator 3 in the same system also experiences a substantial rotor angle escalation, though it exhibits relatively better damping compared to Generator 6. Generators 1, 2, 4, and 5, across both the existing and reconfigured setups, demonstrate superior damping properties, with oscillatory behaviour diminishing over time. Network reconfiguration contributes to improved damping, mitigating excessive rotor angle variations. Generators with suboptimal damping, such as Generator 6 and Generator 3 in the existing setup, are more susceptible to instability. The reconfigured system bolsters overall stability, preventing phase divergence among generators, a factor essential for preserving system synchronism.

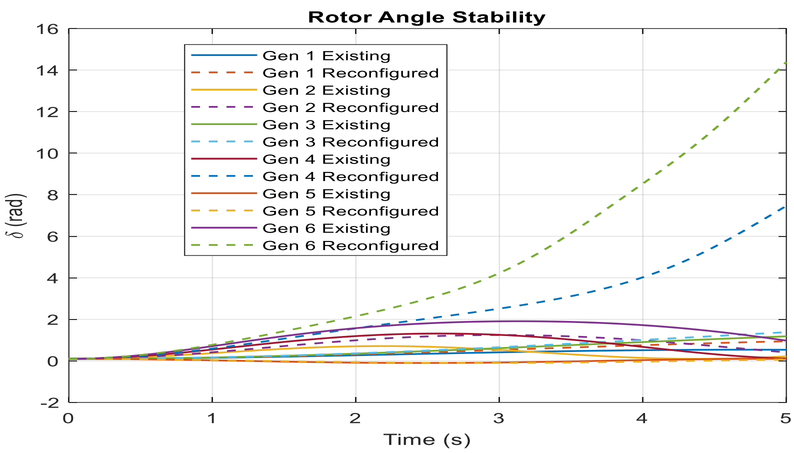

Figure 4: Rotor angle stability of the existing and reconfigured network

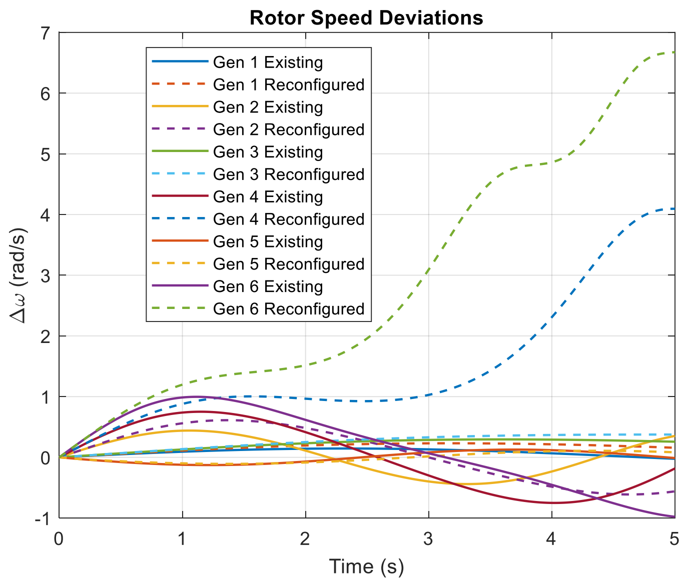

Figure 5: Rotor speed deviation of the existing and reconfigured network

Figure 5 represents the rotor speed deviation of the various synchronous generators of the network. The rotor speed deviations exhibit oscillations, which is typical in response to disturbances in the system. Generator 1 exhibits a moderate initial deviation of approximately 0.5 rad/s, with oscillations that gradually dampen over time, returning close to zero by the 5-second mark in the existing network configuration. In the reconfigured network, the response is similar but with a slightly reduced amplitude and faster damping, indicating enhanced stability. Generator 2 experiences even smaller deviations and exhibits faster damping in the reconfigured system compared to the existing setup. Generator 3 demonstrates poor damping characteristics in the existing system; however, reconfiguration significantly enhances its stability. Generator 4 exhibits good damping performance, with only marginal improvements observed following reconfiguration. Similarly, Generator 5 possesses strong inherent damping properties, which are slightly enhanced in the reconfigured system. Generator 6, on the other hand, undergoes a large initial deviation exceeding 5 rad/s, with oscillations that persist and increase over time, indicating an undamped response and a potential loss of synchronism in the existing system. However, in the reconfigured network, the initial deviation is reduced, and the oscillations dampen effectively, stabilizing near zero by the 5-second mark. These observations highlight severe damping deficiencies in the existing system that may lead to instability, whereas network reconfiguration significantly improves system performance and stability. The findings given herein correspond with the conclusions of [2], which revealed the strategic alterations to the power network to enhance fault response and overall system resilience.

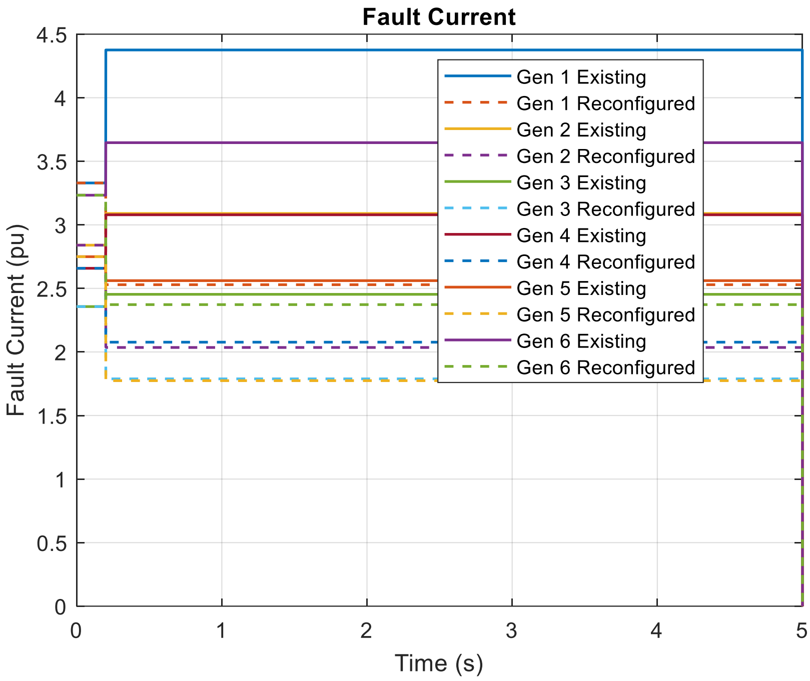

Figure 6: Fault current determination of the existing and reconfigured network

Figure 6 depicts the fault currents for many generators in existing and redesigned networks. Under the existing network configuration, Generator 1 exhibits the highest fault current, exceeding 4.5 pu, indicating a substantial contribution to fault conditions. However, in the reconfigured network, the fault current is significantly reduced to approximately 2.5 pu, demonstrating improved fault-handling capabilities. For Generator 2, the fault current in the existing system is relatively high, around 3.5 pu. Following reconfiguration, this value decreases to approximately 2.0 pu, indicating enhanced protection and improved system resilience. In the case of Generator 3, the fault current in the existing system is around 2.4 pu. Reconfiguration effectively reduces this value to approximately 1.75 pu, mitigating the impact of fault conditions on the generator. Generator 4 initially experiences a fault current of approximately 3.15 pu under the existing configuration. After reconfiguration, a reduction to around 2.1 pu is observed, implying a more stable operational condition. For Generator 5, the existing system exhibits a fault current of around 2.5 pu. The reconfigured network decreases this value to 1.7 pu, contributing to overall system stability. Lastly, Generator 6 experiences an initial fault current of approximately 3.7 pu in the existing system. The reconfigured network effectively reduces this value to around 2.4 pu, suggesting enhanced fault management and improved system performance.

Table 3: Shunt reactor allocation for the reconfigured Southern Nigerian network

Bus Location	Bus Number	Reactor Reactance, X_{Rt}(pu)	Purpose
Benin	2	2.00	Fault current mitigation and damping enhancement
Makurdi	9	2.857	Fault current mitigation and damping enhancement
Lafia	10	4.00	Fault current mitigation and damping enhancement

In table 3, the selected shunt reactors were permanently connected at Benin, Makurdi, and Lafia buses in the reconfigured network configuration. These locations were selected based on their influence on network dynamic behaviour and their ability to improve transient stability performance. The reactor reactance values were incorporated into the network model for the simulation results presented in Figures 4–6 above.

3.3 Sensitivity Analysis

Figure 7 illustrates a graph of fault current (in pu.) over time (in seconds) for varying reactance values (shunt reactors) in the power network. The graph shows the following trends:

At $X_{Rt} = 0.00\, pu.$, the fault current is highest, around 3.0 pu., as zero reactance results in minimal impedance, allowing maximum current flow.

As X_{Rt} increases, the fault current decreases:

$X_{Rt} = 0.05\, p.u.$: Fault current is approximately 2.4 pu.

$X_{Rt} = 0.10\, p.u.$: Fault current is around 2.1 pu.

$X_{Rt} = 0.15\, p.u.$: Fault current is around 1.65 pu.

$X_{Rt} = 0.20\, p.u.$: Fault current is approximately 1.55 pu.

$X_{Rt} = 0.50\, p.u.$: Fault current reduces to about 0.8 pu.

$X_{Rt} = 0.75\, p.u.$: Fault current decrease further to about 0.6 pu.

For all reactance values, the fault current stabilize almost immediately after the fault occurs, indicating a quick system response. The graph highlights an inverse relationship between reactance and fault current: as reactance increases, fault current decreases because added reactance increases total impedance, thereby limiting current flow during faults. While lower reactance may improve system efficiency under normal operating conditions, higher reactance enhances protection by reducing fault currents.

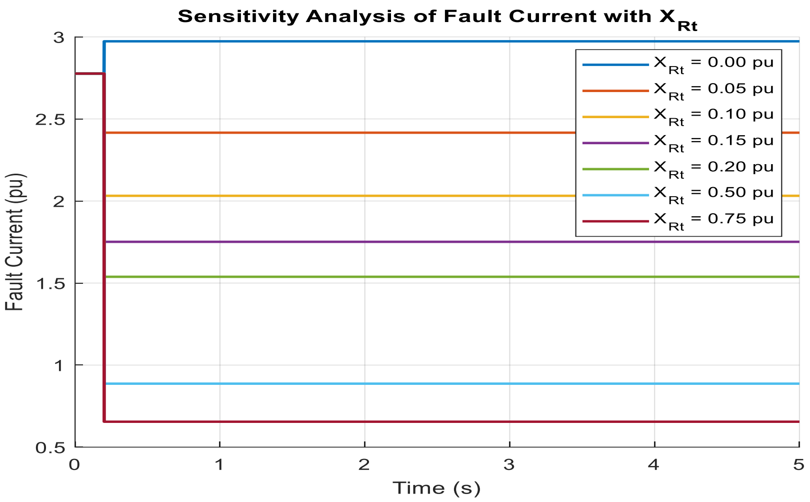

Figure 7: Sensitivity analysis of fault current with shunt reactor

Table 3: Generator parameters of the network

Bus No.	Generator	H(MW.s/MVA)	D	Pm(pu)	X_d'' (pu)	Xt(pu)	Ei(pu)
1	Gen 1	8.2	0	2.3614	0.130	0.00696	1.038
3	Gen 2	1.18	0	2.08	0.160	0.03306	1.033
6	Gen 3	9.62	0	3.007	0.226	0.03899	1.143
11	Gen 4	1.299	0	3.258	0.190	0.01720	1.105
13	Gen 5	1.37	0	0.000	0.164	0.06545	1.000
15	Gen 6	1.37	0	4.631	0.164	0.02620	1.176

Source [16]

Table 4: Transmission line data of the 16-bus network

From Bus	To Bus	R (pu)	X (pu)	B (pu)
1	13	0.0009	0.00696	0.10349
2	3	0.001809	0.013912	0.20698
2	4	0.00491	0.04164	0.52026
2	5	0.003827	0.03249	0.343171
2	6	0.003447	0.029263	0.3665
3	16	0.00226	0.01915	0.23924
4	5	0.00068	0.005769	0.060937
4	7	0.00344	0.02918	0.36456
4	11	0.002025	0.017196	0.21536
4	13	0.00494	0.04194	0.52406
6	16	0.00115	0.00973	0.12152
7	8	0.00025	0.00195	0.02906
8	9	0.005615	0.047673	0.59707
8	12	0.00586	0.04507	0.67251
9	10	0.003623	0.027853	0.415541
12	13	0.001949	0.016549	0.174793
12	15	0.002449	0.020794	0.26043
14	15	0.000637	0.005405	0.06769

Source [16]

4. Conclusion

This study investigates the effects of inertia and damping coefficients on fault current and transient power angle stability within the Southern Nigeria 16-Bus network, incorporating shunt reactors. Steady-state load flow analysis was performed using MATPOWER 8.0. The study also presented a mathematical model for incorporating reactance into the network during a three-phase fault. The results revealed that network reconfiguration enhanced rotor angle stability, rotor speed deviation, fault current, and sensitivity analysis. The reconfiguration improved damping performance of generators of the network. Generators 1, 2, 4, and 5, across both the existing and reconfigured setups, demonstrate superior damping properties, with oscillatory behaviour diminishing over time. Network reconfiguration contributes to improved damping, mitigating excessive rotor angle variations. Generators with suboptimal damping, such as Generator 6 and Generator 3 in the existing setup, are more susceptible to instability. The reconfigured system bolsters overall stability, preventing phase divergence among generators, a factor essential for preserving system synchronism. Additionally, fault current analysis revealed a significant reduction in generator 1 from 4.5 pu. to 2.5 pu. after reconfiguration, while generator 2 experienced a decrease from 3.5 pu. to 2 pu. All generators benefit from reduced rotor angle deviations and improved damping, with Gen 3 and Gen 6 showing the most significant improvements. This suggests that network reconfiguration enhances overall system stability by mitigating excessive rotor speed deviations and preventing phase drift. For the sensitivity analysis, the peak fault current occurs at X_{Rt}=0.00 p.u., where zero reactance minimizes impedance for maximum current flow. As X_{Rt} increases, the fault current decreases gradually, reaching 0.8 pu. at X_{Rt}=0.50 pu. and further decreasing to 0.6 pu. at X_{Rt}=0.75 pu. The findings indicated an inverse relationship between reactance and fault current, where increased reactance reduced fault currents, thereby enhancing system protection. Further research is recommended to implement additional damping devices and simulate the long-term impact of reconfiguration on system stability.

References

[1] D. Otuo-Acheampong, G. I. Rashed, A. A. Mensah and H. Haider, "Three-Phase Fault Analysis of Power System Transient Stability Based on TCSC Controller using FPA for its Location," Journal of Physics: Conference Series, vol. 2467, pp. 1-11, 2023, https://doi:10.1088/1742-6596/2467/1/012014.

[2] N. B. Gautam, N. Poudel, K. C. Bibas, R. Sah, K. R. Neupane, P. Basnet, A. Shah, and B. Pandey, "Transient Stability Analysis of Power System Using ETAP," International Journal of Advanced Engineering, Vol. 06, No. 1, pp. 20-35, 2023.

[3] J. U. Agber, P. E. Odaba and C. O. Onah, "Effect of Power System Parameters on Transient Stability Studies," American Journal of Engineering Research, Vol.4, No. 2, pp. 87-94, 2015.

[4] A. Aziz, M. Z. Yousaf, F. Renhai, W. Khan, U. Siddique, M. Ahmad, M. Abbas, M. Bajaj and I. Zaitsev, "Advanced AI-driven Techniques for Fault and Transient Analysis in High-voltage Power Systems," Scientific Reports, Vol. 15, pp. 1-18, 2025, https://doi.org/10.1038/s41598-025-90055-7

[5] H. Wang, L. Hu, and Y. Zhang, "SVM Based Imbalanced Correction Method for Power Systems Transient Stability Evaluation," ISA Transactions, vol. 136, pp. 245–253, 2023, https://doi: 10.1016/j.isatra.2022.10.039.

[6] R. Zhang, W. Yao, Z. Shi, L. Zeng, Y. Tang, and J. Wen, "A Graph Attention Networks-Based Model to Distinguish the Transient Rotor Angle Instability and Short-Term Voltage Instability in Power Systems," International Journal of Electrical Power and Energy Systems, vol. 137, pp. 1-12, 2022, doi: 10.1016/j.ijepes.2021.107783.

[7] F. Jiashu, L. Chongru, Z. Le, and S. Chenbo, “International Journal of Electrical Power and Energy Systems A data-driven method for online transient stability monitoring with vision-transformer networks,” International Journal of Electrical Power and Energy Systems, vol. 149, pp. 1-10, 2023, doi: 10.1016/j.ijepes.2023.109020.
[8] W. Yang, C. Tu, F. Xiao, and Q. Guo, “International Journal of Electrical Power and Energy Systems A combined regulation method of transient power angle stability control and fault current suppression for VSG,” International Journal of Electrical Power and Energy Systems, vol. 156, pp. 1-15, 2024, doi: 10.1016/j.ijepes.2023.109702.
[9] S. T. Atilola, I. A. Adejumobi, O. I. Adebisi and I. A. Osinuga, “Analysis of Power System Transient Stability of the Nigerian 330-kV Electricity Grid,” FUOYE Journal of Engineering and Technology, Vol. 8, No. 3, pp. 300-306, 2023, http://doi.org/10.46792/fuoyejet.v8i3.105.7
[10] S. L. Braide and E. J. Diema, “Analysis of Steady and Transients-State Stability of Transmission Network,” International Journal of Academic Research and Reflection, Vol. 6, No. 5, pp. 1-32, 2018.
[11] D. Das, “Electrical Power Systems,” New Age International Publishers, pp. 405-411, 2006.
[12] P. Kundur, “Power System Stability and Control,” Power System Engineering Series, McGraw-Hill, Inc., pp. 341-360, 1993.
[13] M. Brezovec, I. Kuzle, and M. Krpan, “Detailed Mathematical and Simulation Model of a Synchronous Generator,” Journal of Energy - Energija, vol. 64, no. 1–4, pp. 102–129, 2022, https://doi:10.37798/2015641-4147
[14] A. S. Umeozulu, I. I. Eneh, and J. I. Aneke, “Enhancing Transient Stability of Nigeria 330kv Transmission Grid Using a High Voltage Direct Current (HVDC),” Iconic Research and Engineering Journals, vol. 5, no. 8, pp. 172-186, 2022.
[15] D. P. Kothari and I. J. Nagrath, "Modern Power System Analysis," Tafe McGraw-Hill Publishers, New Delhi, India, pp.466-468, 2003.
[16] Transmission Company of Nigeria, 2024.